Japanese Journal of Applied Physics

The Japan Society of Applied Physics

ACCEPTED MANUSCRIPT

Low temperature selective growth of Ga-doped and Ga-B Co-doped germanium source / drain for PMOS devices

To cite this article before publication: Clement Porret *et al* 2023 *Jpn. J. Appl. Phys.* in press https://doi.org/10.35848/1347-4065/acb1b9

Low Temperature Selective Growth of Ga-Doped and Ga-B Co-Doped Germanium Source / Drain for PMOS Devices

Clement Porret[1], Gianluca Rengo[1,2,3], Mustafa Ayyad[1], Andriy Hikavyy[1], Erik Rosseel[1], Robert Langer[1], and Roger Loo[1]

[1] imec vzw, Kapeldreef 75, B-3001 Leuven, Belgium
[2] Quantum Solid State Physics, KU Leuven, Celestijnenlaan 200D, B-3001 Leuven, Belgium
[3] FWO - Vlaanderen, Egmontstraat 5, 1000 Brussel, Belgium

Abstract

The peculiarities and physical properties of gallium-doped (Ge:Ga) and gallium and boron co-doped germanium (Ge:Ga:B) epilayers grown at low temperature (320°C) by chemical vapor deposition are investigated and benchmarked against their boron-doped (Ge:B) counterpart. Ge:Ga films with resistivities < 0.3 mΩ.cm are demonstrated, outperforming Ge:B prepared with a similar method. A selective Ge:Ga growth process based on a cyclic deposition and etch routine is developed and applied to fin structures. Full process selectivity towards nitride and oxide surfaces is demonstrated. Ga incorporation is however reduced, compared to non-selective growth, resulting in a degradation of the electrical performance. Ti / Ge:Ga(:B) contacts are finally evaluated, with the aim of providing new solutions for advanced Ge-based devices.

1. Introduction

Achieving very high doping concentrations in group-IV semiconductor materials is of prime importance for the next generations of metal-oxide-semiconductor field-effect transistors (MOSFET). This allows to decrease the contributions from parasitic contact resistances to the devices, which limit the performance at scaled dimensions.[1] Significant efforts have been devoted to maximizing the active doping concentrations in e.g. n-Si[2], p-SiGe[3], and p-Ge[4] source / drain (S/D) materials for n-Si, p-Si(Ge), and p-(Si)Ge MOSFET, respectively.

While B is conventionally used to p-dope (Si)Ge S/D, the interest in Ga has recently been renewed, motivated by the demonstration of record sub-$1x10^{-9}$ $\Omega.cm^2$ specific resistivity (ρ_c) values for Ti contacts deposited on Ga ion-implanted (Si)Ge.[5-6] Benefits from Ga doping are mostly expected in Ge-rich SiGe materials, where its maximum solubility (~ $5x10^{20}$ cm^{-3} in Ge)[7] largely exceeds that of B[8], while exhibiting comparable ionization energies.[9] In addition, the large Ga atomic radius (larger than that of Ge), makes the Ga-doped (Ge:Ga) system attractive as a S/D stressor for p-Ge MOSFET.[10] For these latter devices, issues with Ge reflow and dopants diffusion set an upper limit on the thermal budget possibly applied during S/D epitaxy. For these reasons, processing should occur at limited temperature.[11]

Several reports dealing with the epitaxy of in situ doped Ge:Ga are available in literature. Pioneering works were conducted by Strite et al., who integrated Ge:Ga in AlGaAs / Ge / GaAs heterojunction bipolar transistors using molecular beam epitaxy.[12] Kesan et al. then explored the system more thoroughly in the 450 to 550°C growth temperature range, and demonstrated active doping concentrations approaching ~ $1x10^{20}$ cm^{-3} with box-shaped profiles.[9] Interestingly, they also observed that Ga doping occurred through the presence of an adlayer at the growth front, indicating a surface diffusion limited incorporation of the dopants. Other groups later introduced Ga-doping in GeSn, achieving active doping levels up to ~ $1.2x10^{20}$ cm^{-3} (resistivity ~ 0.5 mΩ.cm) in $Ge_{0.92}Sn_{0.08}$,[13-14] and ~ $1.6x10^{20}$ cm^{-3} in $Ge_{0.95}Sn_{0.05}$.[15] Although the material quality was degraded above those concentrations, low ρ_c values in the low $1x10^{-9}$ $\Omega.cm^2$ regime could be demonstrated.

Huffman and Casey initiated the chemical vapor deposition (CVD) assessment of Ge:Ga by flowing $GeCl_4$ and $GaCl_3$ as Ge and Ga precursors, respectively.[16] The choice of the $GaCl_3$ precursor was motivated by former works done on the Si:Ga system,[17] where the halide precursor prevented risks for unwanted C incorporation,[18] although the C solubility in Ge is extremely low.[19] The method resulted in films with high purity. However, in the range of explored conditions, only low doping levels ([Ga] ≤ $1x10^{17}$ cm^{-3}) could be obtained, likely due to the low vapour pressure of the solid $GaCl_3$ precursor.

Metalorganic (MO) precursors constituted a credible alternative for enabling higher doping levels thanks to higher partial pressures. Considering safer precursors, Jakomin et al. proposed the use of the unconventional iso-butyl germane precursor in combination with trimethylgallium (TMGa). Thick Ge:Ga films could then be grown at 550 and 670°C with free hole densities up to ~ $2x10^{21}$ cm^{-3}.[20] However, defects related to the formation of Ga droplets during deposition were observed when exceeding a concentration of ~ $1x10^{19}$ cm^{-3}. Two options were proposed and validated to avoid the formation and coalescence of Ga-rich clusters: operate at relatively high temperature (670°C), at which superficial Ga in excess can desorb rapidly, or work with limited Ga precursor flows and reduced thermal budgets (550°C), where the importance of diffusion phenomena is reduced. Jin et al. confirmed this statement by suppressing the occurrence of Ga clustering during the epitaxy Ge:Ga on GaAs using germane (GeH_4) and TMGa thanks to an increase in growth temperature.[21] Finally, Xu et al. broke the $2x10^{20}$ cm^{-3} active concentration wall in defect-free Ge:Ga by taking advantage of

CVD reactions between tetragermane (Ge_4H_{10}) and dimethylamine-gallane ($[D_2GaN(CH_3)_2]_2$).[22] The reaction yielded epitaxial films with nearly full doping activation up to $2.7x10^{20}$ cm^{-3} (resistivity ~ 0.4 mΩ.cm) at temperatures as low as 360°C, undeniably providing a step forward in the quest for highly doped Ge:Ga. However, the proposed precursors are not standardly available and the method is, at the moment, not scalable to large production.

In this manuscript, commercial precursors are instead considered, following preliminary works done on the SiGe:B(:Ga) material system with other precursors.[23-24] The work was introduced in an extended SSDM abstract[25] and takes advantage of the cyclic deposition-etch (CDE) method previously described in the case of Ge:B epilayers[4] to develop selective growth conditions for Ge:Ga. With respect to the previous report, additional background information regarding the Ga precursor selection and experimental conditions are provided. The physical properties of Ge:Ga layers deposited with standard and selective growth conditions are discussed in more detail. The resulting Ga chemical concentration profiles are e.g. compared, which allows to identify some limitations of the proposed process. Early results from Ga-B co-doping are also presented.

First, the physical properties of the grown Ge:Ga materials are evaluated. Selective epitaxial growth (SEG) conditions are demonstrated on Ge fins with SiN_x spacers. Next, the limitations associated to the SEG process performance are discussed. Finally, the co-doping with Ga and B is addressed as a potential way to further boost the material electrical properties. A first assessment of Ti / Ge:Ga(:B) contact properties is proposed, using the multi-ring circular transmission line method (MR-CTLM) introduced earlier.[26] This study constitutes a first evaluation of the new possibilities offered by Ga doping for the performance improvement of Ge-based devices.

2. Process description

The epitaxial films presented in this work were grown by reduced-pressure CVD at a growth temperature of 320°C, using digermane (Ge_2H_6) and tri-tertiary-butylgallium (TTBGa) as Ge and Ga precursors, respectively. TTBGa was selected amongst other commercially available MO precursors, listed in Table 1, considering trends extracted from literature reports dealing with the epitaxy of III-V materials.[27] Note that TMGa, TEGa and TTBGa are liquid precursors and require bubbler delivery systems. $GaCl_3$ is a solid source[16]. In comparison with TMGa and triethylgallium (TEGa), TTBGa is expected to provide several advantages. It indeed features a lower decomposition temperature,[28] thereby enabling doping at lower growth temperatures. It also exhibits a larger steric hindrance and a reduced Ga-C bond stability (thanks to the β-hydride elimination mechanism),[29] which is expected to limit C incorporation.[29-30] It finally provides a vapor pressure suitable for most doping applications. B_2H_6 was added to the growth chemistry to study Ga-B co-doping.

Table 1. Characteristics of several Ga precursors.

Precursor	Chemical Formula	Molecular mass (g/mol)	Vapor pressure at 20°C (Torr)
Trimethyl-gallium (TMGa)	$Ga(CH_3)_3$	114.8	~ 180
Triethyl-gallium (TEGa)	$Ga(C_2H_5)_3$	156.9	~ 5
Tri-tertiary-butyl-Gallium (TTBGa)	$Ga(C(CH_3)_3)_3$	241.1	~ 1
Gallium trichloride	$GaCl_3$	176.1	~ 0.1

The growth experiments were performed on 600 nm thick mildly As-doped (~ $1x10^{17}$ cm^{-3}) Ge virtual substrates (VS) at reduced pressure and a setpoint temperature of 320°C (Fig. 1(a)).[4] It may be important to note that this nominal temperature was measured by thermocouples positioned on the backside of the susceptor holding the wafer and may be lower than the actual surface temperature. Low temperature processing was preferred in view of maximizing Ga incorporation while preventing its segregation. As the considered low temperature epitaxy process is non-selective, it was combined with a selective etching using Cl_2 in a reproducible isothermal and isobaric CDE routine. Tuning the deposition and etch durations allowed to setup conditions avoiding the deposition of polycrystalline Ge grains on Si oxide and nitride surfaces present on wafers patterned with Ge fins (Fig. 1(b) and Fig. 2).

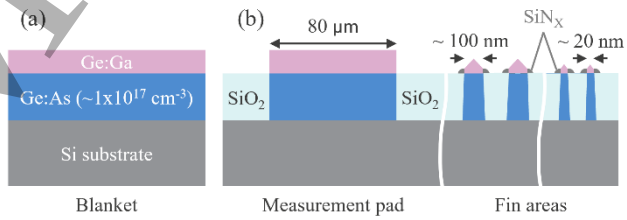

Fig. 1. Schematics describing the growth experiments performed on (a) Ge:As virtual substrates and (b) wafers patterned with Ge fins, including 80 x 80 $µm^2$ measurement pads and areas with fins of different dimensions.

Adjusting the number of CDE cycles allowed to obtain the desired material thickness. The grown epi materials were characterized by differential mass measurements and X-ray reflectivity (for thickness extraction), top view scanning electron microscopy (SEM, for morphology evaluation), secondary ion mass spectrometry (SIMS, for compositional analysis), micro-4-point-probe and micro-Hall effect (MHE) measurements (for electrical assessment).

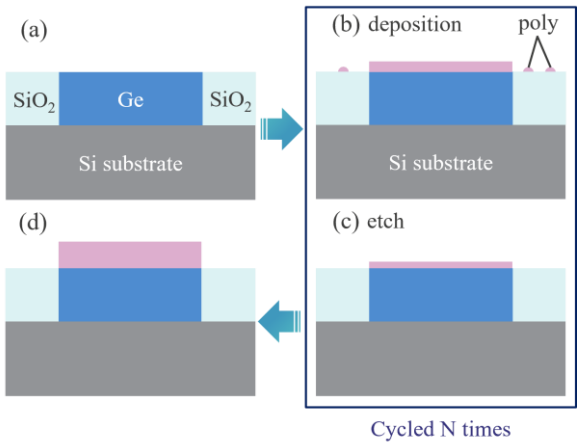

Fig. 2. Schematic illustration of the processing steps composing the cyclic deposition-etch routine in the case of a measurement pad: (a) the patterned wafer is introduced in the CVD reactor and the native oxide desorbed in situ. (b) Several nm of Ge:Ga are deposited, resulting in epitaxial growth in the Ge window and the formation of polycrystalline Ge grains on the surrounding Si oxide surfaces. (c) The deposition is stopped and Cl_2 is flown to fully etch the polycrystalline grains. The mono-crystalline Ge:Ga is only partially etched. (d) Repeating steps (b) and (c) in a cyclic manner allows to obtain the selective deposition of Ge:Ga on Ge.

3. Physical properties of the grown Ge:Ga epi layers

In an early contribution,[31] Ge:Ga was successfully grown with flat Ga profiles and active doping levels exceeding $1x10^{20}$ cm^{-3} (resistivity < 0.4 mΩ.cm). However, keeping Ga diluted in the Ge matrix and avoiding clustering was identified as a challenge. In this manuscript, we demonstrate materials with controlled defectivity and resistivity < 0.3 mΩ.cm. Table 2 summarizes some of the main physical properties of 3 selected Ge:Ga samples grown with different TTBGa flows. The TTBGa flows are given in arbitrary units (a.u.) since the exact mass flow rates (e.g. in mg/min), function of the vessel temperature and carrier gas flown through the bubbler, are unknown. Fig. 3 displays the corresponding top-view SEM inspections.

Table 2. Growth rate and electrical properties of 3 Ge:Ga epilayers grown with different TTBGa flows (F). $[Ga]_{act}$ is estimated by MHE assuming a Hall scattering factor (HSF) of 1. Estimated error bars are provided. *The error bars on $[Ga]_{act}$ will be much larger in case we consider possible errors on HSF.

ID	F (a.u.)	GR (nm/min)	$\rho_{Ge:Ga}$ (Ω.cm)	μ_H ($cm^2.V^{-1}.s^{-1}$)	$[Ga]_{act}$ (cm^{-3})	$[Ga]_{chem}$ (cm^{-3})
A	1	7.9	$5.5x10^{-4}$	61	$1.9x10^{20}$	$1.4x10^{20}$
B	2.5	6.8	$2.8x10^{-4}$	33	$6.6x10^{20}$	$3.6x10^{20}$
C	5	6.2	$2.6x10^{-4}$	33	$7.3x10^{20}$	$3.3x10^{20}$
Est. error +/-		3%	5%	3	10%*	10%

Sample A (Fig. 3(a)) is a 63 nm thick Ge:Ga layer grown with TTBGa flow F_1 = 1 a.u. and characterized by a growth rate (GR) of ~ 7.9 nm/min. It exhibits a smooth surface and a resistivity $\rho_{Ge:Ga}$ of 0.55 mΩ.cm. The active doping concentration ($[Ga]_{act}$), estimated from MHE assuming a Hall scattering factor (HSF) of 1, amounts to $1.9x10^{20}$ cm^{-3}. The extracted Hall carrier mobility is μ_H = 61 $cm^2.V^{-1}.s^{-1}$. The estimated $[Ga]_{act}$ exceeds the chemical Ga concentration ($[Ga]_{chem}$) of $1.4x10^{20}$ cm^{-3} extracted by SIMS. A best assumption therefore is that most of the Ga dopants present in the sample are electrically active. This is supported by X-ray absorption fine structure measurements, performed on similar samples and combined with density functional theory analysis, reported in [32]. Those indeed indicated that the majority of the Ga impurities were occupying substitutional sites in the Ge matrix. A full activation of the dopants can however not be confirmed due to a lack of literature reports on HSF values for high doping levels. This result nevertheless suggests that the HSF cannot be larger than 0.74, as the electrically active doping concentration cannot exceed the chemical doping concentration.

As expected, $[Ga]_{chem}$ and $[Ga]_{act}$ increase with increasing the TTBGa precursor flow. Sample B (Fig. 3(b)), grown with TTBGa flow F_2 = 2.5 a.u., is a bit thinner and has a resistivity as low as 0.28 mΩ.cm. $[Ga]_{chem}$ amounts to $3.6x10^{20}$ cm^{-3}, one of the highest doping levels reported so far. For this sample, the HSF is necessarily ≤ 0.55, with $[Ga]_{act}$ = $6.6x10^{20}$ cm^{-3} and μ_H = 33 $cm^2.V^{-1}.s^{-1}$. The observed decrease in Hall mobility, dominated by Coulomb scattering, supports an increase in active doping.

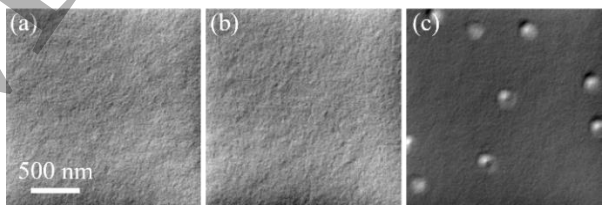

Fig. 3. Top-view SEM presenting the surface morphologies of three Ge:Ga epi layers grown with different TTBGa flows, all conditions being the same otherwise. Samples grown with (a) low TTBGa flow F_1, (b) TTBGa flow F_2 = 2.5 F_1 and (c) TTBGa flow F_3 = 5 F_1.

Beyond TTBGa flow F_2, Ga clustering cannot be prevented. Sample C (Fig. 3(c)), grown with TTBGa flow F_3 = 5 a.u., exhibits surface defects identified as Ga-rich clusters. A critical TTBGa partial pressure for cluster formation in these growth conditions is therefore determined. Saturations in $\rho_{Ge:Ga}$, $[Ga]_{chem}$, $[Ga]_{act}$, and μ_H are observed.

4. Selective Ge:Ga growth on fins

Cl_2 etching steps were introduced in the deposition process and the resulting CDE routine applied to Ge fins with nitride spacers and separated by SiO_2 shallow trench isolation to confirm process selectivity (Fig. 1(b)). Net growths per cycle of ~ 3 and 3.5 nm were obtained on blanket Ge and pads present on fin wafers, respectively (Fig. 4). As observed on samples A, B and C (epi only), the growth rate on blanket

wafers decreases with increasing the TTBGa flow. The trend is modified on fin wafers, where the net growth per cycle is enhanced due to loading effects. Moreover, for the given process conditions, it remains approximately constant until a critical TTBGa flow of ~ 4 a.u. is reached. It then decreases sharply, indicating a faster etching rate on materials with higher doping.

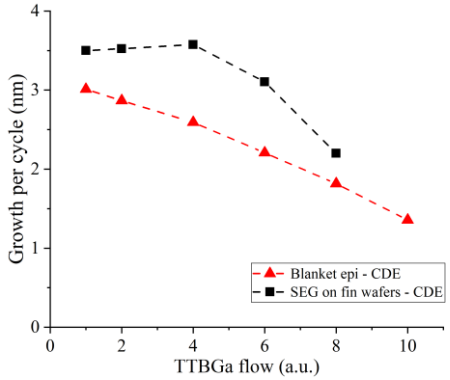

Fig. 4. Growth per cycle as a function of TTBGa flow for CDE processes applied to blanket Ge (red triangles) and fin wafers (black squares).

Fig. 5 presents SEM inspection results after Ge:Ga SEG on Ge fins. Two different CDE recipes, with low (4 a.u., Fig. 5(a-b)) and high (10 a.u., Fig. 5(c-d)) TTBGa flows, result in SEG towards the oxide and nitride surfaces present on the test wafers. The materials grown with the low TTBGa flow exhibit smooth surfaces on both wide (Fig. 5(a)) and narrow (Fig. 5(b)) fins. However, exceeding the critical TTBGa precursor flow causes a roughening of the Ge:Ga films deposited on metrology pads (not shown here). Such conditions also prevent Ge:Ga from growing on narrow fins (Fig. 5(d)). The proximity of nitride and oxide surfaces indeed induces material faceting at the sidewall interface[33], which causes stress and enhanced epi defectivity on slow-growing {111} or {113} crystallographic planes.[34]

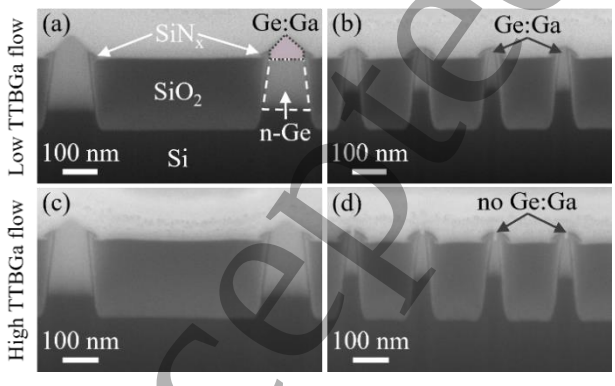

Fig. 5. Cross-section SEM from (a-c) wide and (b-d) narrow fins after the Ge:Ga SEG with (a-b) low and (c-d) high TTBGa flows.

The CDE routine also affects the electrical properties. Fig. 6 shows the evolution of material resistivity as a function of TTBGa flow for Ge:Ga layers grown without and with the CDE process. For a given TTBGa flow, implementing the CDE results in a significant increase in resistivity. This is explained by a reduced Ga incorporation, as confirmed by SIMS in Fig. 7.

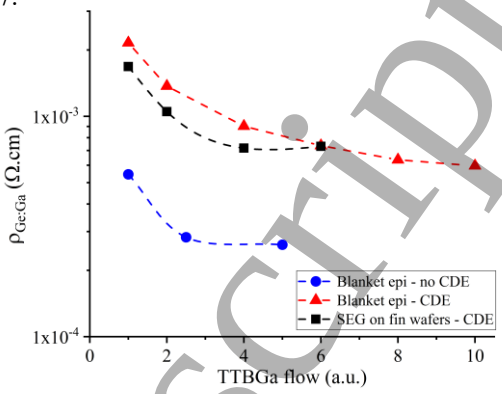

Fig. 6. Ge:Ga bulk resistivity as a function of TTBGa flow used during growth, in the case of blanket epi without Cl_2 (blue circles), blanket epi with Cl_2 etching steps (red triangles) and the CDE procedure applied to fins wafers (black squares).

For a Ge:Ga layer grown with a TTBGa flow of 4 a.u., employing the CDE routine suppresses up to ~ 85% of the incorporated Ga, likely consumed under the form of $GaCl_3$ by-products during growth. $[Ga]_{chem}$ ~ $7x10^{19}$ cm^{-3} remain present in the film. MHE measurements do not indicate any deactivation of these residual Ga dopants. Solutions clearly need to be identified to restore Ga incorporation up to competitive levels. Using higher TTBGa flows to compensate for the loss allows to incorporate up to $[Ga]_{chem}$ ~ $1.5x10^{20}$ cm^{-3} using CDE (not shown here). This is however not an option in view of growth on patterned structures, since higher TTBGa flows lead to low growth rates and even no deposition on narrow fins, as seen in Fig. 5. Extending the Cl_2 purging time between two consecutive etch and deposition steps may nevertheless enhance the achievable Ga doping levels by limiting interactions between Ga and Cl species.

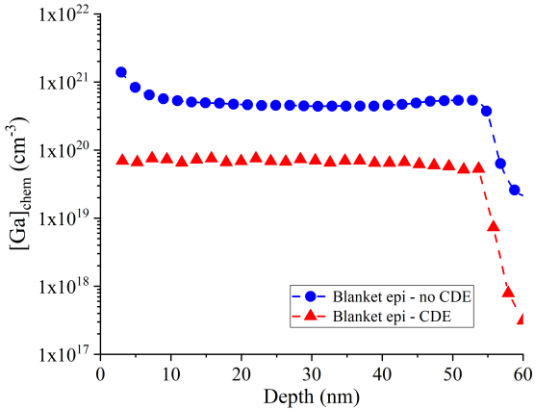

Fig. 7. Chemical Ga concentration profiles extracted from 2 Ge:Ga grown with a TTBGa flow of 4 a.u., without (blue dots) and with (red triangles) the CDE routine.

5. Ga-B co-doping in Ge

Another approach consists in co-doping the Ge layer with Ga and B. Combining two dopants may enable higher active doping concentrations, thanks to strain compensation effects and/or by limiting doping deactivation by, e.g., suppressing free vacancies in the host matrix.[35] A preliminary assessment of the non-selective growth of Ge:Ga:B was therefore conducted.

A reference Ge:B epilayer resulted being ~ 88 nm thick with a resistivity ~ 0.55 mΩ.cm. $[B]_{act}$, estimated using MHE assuming HSF = 1, yielded ~ $1.1x10^{20}$ cm^{-3} (μ_H = 102 $cm^2.V^{-1}.s^{-1}$). Ga was then introduced to grow Ge:Ga:B in similar conditions (all other parameters kept same). The layer was then slightly thinner, ~ 83 nm thick, with a similar *apparent* resistivity ~ 0.54 mΩ.cm. $[Ga+B]_{act}$ was estimated ~ $1.4x10^{20}$ cm^{-3} (μ_H = 78 $cm^2.V^{-1}.s^{-1}$). No morphology degradation was observed.

SIMS measurements were performed to access the B and Ga concentration profiles throughout the layers. Results are presented in Fig. 8. The Ge:B epilayer features a box-like B doping profile with a flat B level of $[B]_{chem}$ = $4x10^{20}$ cm^{-3}. The Ga level is found to be lower than the SIMS detection limit. The activation level $[B]_{act}/[B]_{chem}$ is estimated to be ~ 27%. The Ge:Ga:B layer, however, features a different B profile, with a monotonic decrease from $[B]_{chem}$ = $4x10^{20}$ down to $6x10^{19}$ cm^{-3} towards the sample surface. This phenomenon is assumed to be due to competitive reactions for B and Ga incorporation at the surface of the sample during growth. In the first few nm, B incorporates normally and reaches the same level as in the Ge:B sample. Ga incorporation is delayed and takes off after a Ge thickness of 5-7 nm. As discussed in [9,32] Ga indeed first accumulates at the sample surface before it starts incorporating in the growing layer. The surface is then partly occupied, which apparently decreases the B incorporation efficiency. Consequently, the Ga signal increases towards the surface to saturate around $[Ga]_{chem}$ = $9x10^{19}$ cm^{-3}, while B incorporation reduces significantly. The activation level $[Ga+B]_{act}/[Ga+B]_{chem}$ could be estimated by integrating the total dopant dose in the sample, and resulted being close to 60%.

These results however suffer from significant error bars (due to the non-ideal profiles in Ge:Ga:B and HSF values which can differ for B and Ga dopants) which prevent from drawing conclusions on a possible increase in hole active doping concentration in p-doped Ge thanks to co-doping. Additional investigations are needed to clarify this point. Moreover, the impact of Ga-doping on the resulting B concentration profile suggests the occurrence of complex interactions between the dopant adatoms and/or precursors during surface reactions. These learnings will be leveraged for the design of future studies and process developments.

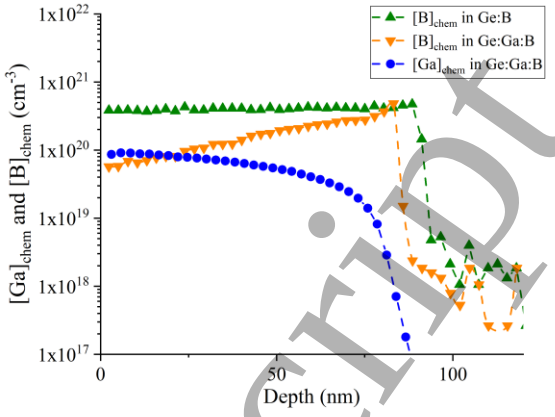

Fig. 8. Chemical Ga and B concentration profiles extracted from a reference Ge:B epilayer ($[B]_{chem}$ in Ge:B, green triangles) and a similar material grown in presence of Ga precursor ($[Ga]_{chem}$ in Ge:Ga:B, orange triangles and $[B]_{chem}$ in Ge:Ga:B, blue dots).

6. Ti / Ge:Ga:B contact resistivity assessments

The specific resistivity (ρ_c) of metal to S/D contacts is an important metric characterizing their performance. Some of the developed materials were therefore used for blanket contact studies.

ρ_c values down to $3.1x10^{-9}$ Ω.cm^2 were e.g. extracted from Ti / Ge:Ga contacts based on non-optimized Ge:Ga epilayers with bulk resistivity down to 0.55 mΩ.cm. Similar tests were conducted with Ti / Ge:Ga:B and confirmed cumulative effects from moderate (< 8 $x10^{19}$ cm^{-3}) Ga-B co-doping in comparison to samples with one single dopant. For instance, Ti contacts formed on Ge:Ga (~ $1x10^{19}$ cm^{-3}, $\rho_{Ge:Ga}$ = 2.10 mΩ.cm) grown with TTBGa flow F_{Ga}, and Ge:B ($[B]_{act}$ ~ $6x10^{19}$ cm^{-3}, $\rho_{Ge:B}$ = 0.80 mΩ.cm) grown with B_2H_6 flow F_B, led to $\rho_c > 1x10^{-8}$ Ω.cm^2. Corresponding contacts to non-optimized Ge:Ga:B ($\rho_{Ge:Ga:B\text{-}apparent}$ = 0.49 mΩ.cm) grown with TTBGa and B_2H_6 flows F_{Ga} and F_B yielded ρ_c ~ $4.8x10^{-9}$ Ω.cm^2. Further investigations in the high doping regime are required to assess the ultimate contact resistivity scaling achievable with this method.

In the end, the reported Ti / Ge:Ga(:B) contacts do not outperform Ti / Ge:B stacks ($\rho_c < 3x10^{-9}$ Ω.cm^2 in[4], down to ~ $2x10^{-9}$ Ω.cm^2 in this new study). Nevertheless, the extracted contact resistivities enter the low $1x10^{-9}$ Ω.cm^2 regime, which demonstrates some potential for Ga-doping in Ge in view of S/D applications in Ge-based devices.

7. Conclusions

This paper summarizes the development of low temperature, highly doped and selectively grown Ge:Ga source / drain materials, using a cyclic routine compatible with advanced device geometries. Ge:Ga films with box-shaped doping profiles and bulk resistivities < 0.3 mΩ.cm are achieved, which outperforms the best Ge:B materials prepared with a similar method. Although the specific resistivity of Ti / Ge:Ga contacts is not yet as low as that of Ti / Ge:B stacks, epi materials

presented in this work remain attractive for Ge PMOS devices. The main challenge ahead is to overcome the limitations linked to the selective implementation of the developed materials. Solutions based on Ga-B co-doping may have potential to overcome these difficulties.

Acknowledgements

The authors express their appreciation to local authorities, the imec core program members and pilot line. Air Liquide Advanced Materials is acknowledged for providing Ge_2H_6. The TTBGa MO precursor is from Dockweiler Chemicals GmbH. All epitaxial materials were grown in an ASM Intrepid™ CVD reactor. Gianluca Rengo received a PhD grant from the Flemish Research Foundation (FWO). This project received funding from the ECSEL Joint Undertaking (JU) under grant agreement No 875999. The JU receives support from the European Union's Horizon 2020 research and innovation programme and Netherlands, Belgium, Germany, France, Austria, Hungary, United Kingdom, Romania, Israel.

References

[1] P. Raghavan, M. Garcia Bardon, D. Jang, P. Schuddinck, Dmitry Yakimets, J. Ryckaert, A. Mercha, N. Horiguchi, N. Collaert, A. Mocuta, D. Mocuta, Z. Tokei, D. Verkest, A. Thean, and A. Steegen, *Proc. Cust. Integr. Circuits Conf.* 2015, 1–5 (2015).

[2] E. Rosseel, C. Porret, A. Hikavyy, R. Loo, M. T., B. Douhard, O. Richard, N. Horiguchi, and R. Khazaka, *ECS Trans.*, **98** (5), 37 (2020).

[3] G. Rengo, C. Porret, A. Hikavyy, E. Rosseel, G. Pourtois, A. Vantomme, and R. Loo, *ECS Trans.*, **98** (5), 27 (2020).

[4] C. Porret, A. Vohra, N. Nakazaki, A. Hikavyy, B. Douhard, J. Meersschaut, J. Bogdanowicz, E. Rosseel, G. Pourtois, R. Langer, and R. Loo, *Phys. Status Solidi A*, 1900628 (2019).

[5] J.-L. Everaert, M. Schaekers, H. Yu, L.-L. Wang, A. Hikavyy, L. Date, J. del Agua Borniquel, K. Hollar, F. A. Khaja, W. Aderhold, A. Mayur, J. Y. Lee, H. van Meer, Y.-L. Jiang, K. De Meyer, D. Mocuta, and N. Horiguchi, *Dig. Tech. Pap. - Symp. VLSI Technol.*, T214 (2017).

[6] L.-L. Wang, H. Yu, M. Schaekers, J.-L. Everaert, A. Franquet, B. Douhard, L. Date, J. del Agua Borniquel, K. Hollar, F. Adeni Khaja, W. Aderhold, A. Mayur, J. Young Lee, H. van Meer, D. Mocuta, N. Horiguchi, N. Collaert, K. De Meyer, and Y.-L. Jiang, *IEEE Intern. Electr. Dev. Meeting (IEDM)*, pp. 22.4.1. (2017).

[7] F. Trumbore, *The Bell Lab tech. J.*, 39 (1), 205 (1960).

[8] S. Uppal, and A. Willoughby, *J. of Appl. Phys.*, **96**, p 1376 (2004).

[9] V. P. Kesan, S. S. Iyer, and J. M. Cotte, *Appl. Phys. Lett.*, **59** (7), 852 (1991).

[10] E. Capogreco, L. Witters, H. Arimura, F. Sebaai, C. Porret, A. Hikavyy, R. Loo, A. Milenin, G. Eneman, P. Favia, H. Bender, K. Wostyn, E. Dentoni Litta, A. Schulze, C. Vrancken, A. Opdebeeck, J. Mitard, R. Langer, F. Holsteyns, N. Waldron, K. Barla, V. De Heyn, D. Mocuta, and N. Collaert, *IEEE Trans. on Electr. Dev.*, **65** (11), 5145 (2018).

[11] R. Loo, H. Arimura, D. Cott, L. Witters, G. Pourtois, A. Schulze, B. Douhard, W. Vanherle, G. Eneman, O. Richard, P. Favia, J. Mitard, D. Mocuta, R. Langer, and N. Collaert, *ECS J. of Sol. State Sci. and Techn.*, **7** (2), P66 (2018).

[12] S. Strite, M. S. Unlu, K. Adomi, G.-B. Gao, and H. Morkoc, *IEEE Trans. on Electr. Dev.*, **11** (5), 233 (1990).

[13] Y. Shimura, S. Takeuchi, O. Nakatsuka, B. Vincent, F. Gencarelli, T. Clarysse, W. Vandervorst, M. Caymax, R. Loo, A. Jensen, D. H. Petersen, and S. Zaima, *Thin Solid Films*, **520** (8), 3206 (2012).

[14] W. Wang, S. Vajandar, S. L. Lim, Y. Dong, V. R. D'Costa, T. Osipowicz, E. S. Tok, and Y.-C. Yeo, *J. of Appl. Phys.*, **119**, 155704 (2016).

[15] Y. Wu, S. Luo, W. Wang, S. Masudy-Panah, D. Lei, G. Liang, X. Gong, and Y.-C. Yeo, *J. Appl. Phys.*, **122**, 224503, (2017).

[16] J. E. Huffman, and N. L. Casey, *J. of Cryst. Growth*, **129** (3-4), 525 (1993).

[17] J. E. Huffman, *J. of Cryst. Growth*, **87** (4), 425 (1988).

[18] P. Rai-Choudhuy, *J. of Cryst. Growth*, **8** (2), 165 (1971).

[19] R.W. Olesinski, and G. J. Abbaschian, *Bul. of Alloy Phase Diag.*, **5** (5), 484 (1984).

[20] R. Jakomin, G. Beaudoin, N. Gogneau, B. Lamare, L. Largeau, O. Mauguin, and I. Sagnes, *Thin Solid Films*, 519 (13), 4186 (2011).

[21] Y. J. Jin, C. K. Chia, H. Liu, L. Wong, J. Chai, D.Z. Chi, and S. Wang, *Applied Surface Science*, **376**, 236 (2016).

[22] C. Xu, P. M. Wallace, D. A. Ringwala, J. Menéndez, and J. Kouvetakis, *ACS Applied Materials & Interfaces*, **10** (43), 37198 (2018).

[23] J. Margetis, D. Kohen, C. Porret, L. Petersen Barbosa Lima, R. Khazaka, G. Rengo, R. Loo, J. Tolle, and A. Demos., *1st Joint International SiGe Technology and Device Meeting (ISTDM) / International Conference on Silicon Epitaxy and Heterostructures (ICSI)*, p. 143 (2018).

[24] C. Porret, A. Hikavyy, J. F. Gomez Granados, S. Baudot, A. Vohra, B. Kunert, B. Douhard, J. Bogdanowicz, M. Schaekers, D. Kohen, J. Margetis, J. Tolle, L. Petersen Barbosa Lima, A. Sammak, G. Scappucci, E. Rosseel, R. Langer, and R. Loo, *ECS Trans.*, **86** (7), 163 (2018).

[25] C. Porret, G. Rengo, M. Ayyad, A. Hikavyy, E. Rosseel, R. Langer, and R. Loo, *Ext. Abstr. of the 2022 Int. Conf. on Solid State Devices and Materials*, p. 469 (2022).

[26] H. Yu, M. Schaekers, T. Schram, E. Rosseel, K. Martens, S. Demuynck, N. Horiguchi, K. Barla, N. Collaert, and K. De Meyer, *IEEE Electron Device Letters*, **36** (6), 600 (2015).

[27] C. Plass, H. Heinecke, O. Kayser, H. Lüth and P. Balk, *J. of Cryst. Growth*, **74** (2), 292 (1986).

[28] M. Yoshida, H. Watanabe and F. Uesugi, *Semicond. Holes*, 132 (3), 677 (1985).

[29] N. Pütz, H. Heinecke, M. Heyen, P. Balk, M. Weyers and H. Lüth, *J. of Cryst. Growth*, 74 (2), 292 (1986).

[30] A. Saxler, D. Walker, P. Kung, X. Zhang, M. Razeghi, J. S. Solomon, W. C. Mitchel and H. Vydyanath, *Appl. Phys. Lett.*, 71 (22), 3272 (1997).

[31] C. Porret, J. Margetis, J. Tolle, A. Sammak, G. Scappucci, L. Petersen Barbosa Lima, D. Kohen, B. Kunert, A. Hikavyy, and R. Loo, *1st Joint International SiGe Technology and Device Meeting (ISTDM) / International Conference on Silicon Epitaxy and Heterostructures (ICSI)*, p. 59 (2018).

[32] G. Rengo, C. Porret, A. Hikavyy, G. Coenen, M. Ayyad, R. J. H. Morris, S. Pollastri, D. Oliveira De Souza, D. Grandjean, R. Loo, and A. Vantomme, *ECS Trans.*, **109**, 249 (2022).

[33] R. Loo, M. Caymax, I. Peytier, S. Decoutere, N. Collaert, P. Verheyen, W. Vandervorst, and K. De Meyer, *J. of The Electrochem. Soc.,* **150** (10), G638 (2003)

[34] P. J. Schubert and G. W. Neudeck, Tech. Reports of Purdue University, (1990) https://docs.lib.purdue.edu/ecetr/719/

[35] A. Vohra, A. Khanam, J. Slotte, I. Makkonen, G. Pourtois, C. Porret, R. Loo, and W. Vandervorst, *J. Appl. Phys.*, **125**, 225703 (2019).